

According to the project proposal, the following objectives have been solved in the stage V/2016:

O1/ Advanced characterization of CoNi/SBA-15 materials.

A1.1. Characterization of reducibility, thermostability and the nature of active sites of CoNi/SBA-15 materials.

In the stage IV/2015 of this project, the physico-chemical properties of the oxide forms of materials of CoNi/SBA-15 type, with different mass ratios between the two transition metals, were investigated. Among the methods of characterization proposed for the investigation of these materials, the XPS method was included in order to explore the composition and the nature of surface species formed after calcination. Due to some technical problems, some results were not included in the previous report and therefore are shown and discussed in the frame of this report.

According to the proposed objectives for the last stage of the project, i.e., V/2016, the investigations on the synthesized solids were mainly focused on the reducibility of metallic cations, the nature of catalytically active metal centers and on their stability at high temperatures. The results of such investigations are very useful to explain the catalytic data and to understand the behavior of these materials during the chemoselective hydrogenation of cinnamaldehyde. In this context, the present report includes results from the thermo-programmed reduction analysis (*TPR*), as well as the data of *in situ* X-ray diffraction– after thermo-programmed reduction (*in situ XRD*), and transmission electron microscopy (*TEM*). Finally, the results of catalytic experiments for the liquid phase hydrogenation of cinnamaldehyde at various hydrogen pressures will be presented.

Selection of the most important results.

Fig. 1 shows some XPS spectra of Co2p and Ni2p that are illustrative for the bi-component solids - based on cobalt and nickel - prepared and investigated in this project. According to the literature data, the value of binding energy of 854.9 eV is attributed to Ni2p in NiO. After curves fitting, the experimental values obtained for samples containing nickel are greater than the mentioned value, i.e., 854.9 eV, (Table 1),

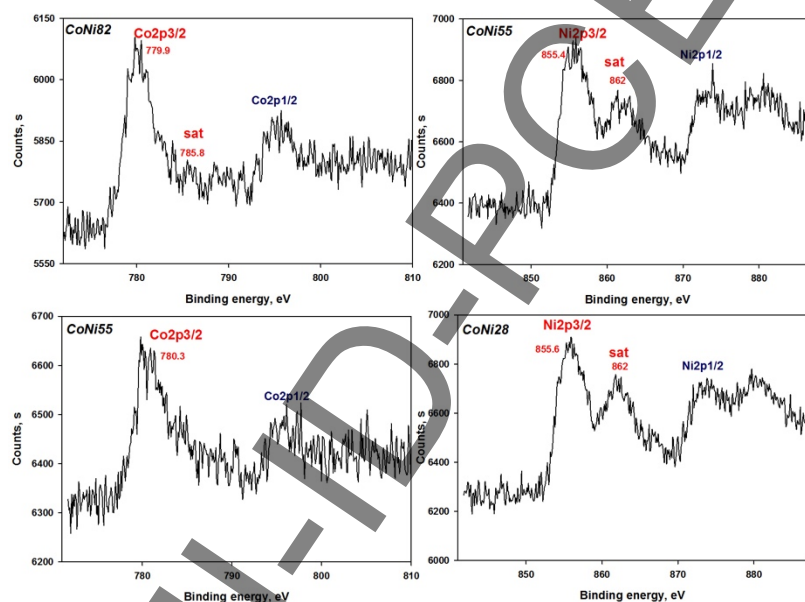


Fig. 1. XPS spectra of Co2p (left) and Ni2p (right) for calcined CoNi/SBA-15.

and in agreement to the XRD analysis at small angles (see Fig. 1 from the report of the stage IV/2015), the Co2p spectra from Fig. 1 - corresponding to samples CoNi82 and CoNi55 - are attributed to the oxide form of type Co_3O_4 resulted on the silica surface during the calcination process. As expected, the satellite peak of sample CoNi82 is less contoured than in the case of sample CoNi55, feature which could be correlated with the concentration of Co_3O_4 existing in this sample. Moreover, after spectra fitting for Co2p of these samples, the values of binding energy for Co2p (Table 1) are similar to those obtained for Co loaded on silica (i.e., 780.5 eV), value which is intermediate between those corresponding to the species Co^{3+} and Co^{2+} .² Note that the ratio M/Si is much smaller at solid

suggesting strong interaction between nickel atoms and silica support. Obviously, such high values of binding energy are indicative for the formation of nickel-phyllsilicates of type 1:1¹. XPS spectrum for Co^{2+} shows a main peak centered at ~ 779.0 eV with a satellite at ~ 786.0 eV. In the case of Co_3O_4 , the spectrum should show both peaks due to the simultaneously presence of Co^{2+} and Co^{3+} cations, but this condition is fulfilled depending on the concentration of Co_3O_4 present in the sample, as this concentration is smaller the contribution of satellite peak is smaller. On the other side, the main peak has an allure more symmetrically than those of Co^{2+} (e.g. for CoO). Taking into account these data, and

surface than in the bulk (Table 1), which indicates a preferential localization of the Co- and/or Ni-based nanoparticles inside of mesopores of SBA-15 silica support, thus confirming the data provided by other methods of characterization.³ It can be concluded that at the surface of the bi-component materials of type CoNi/SBA-15, cobalt and nickel are not involved in mixed compounds of spinels type as it was observed from the analysis in bulk by XRD, and rather forming mono-component species of Co₃O₄ type and Ni-phyllosilicate, respectively, without interactions between them.

Table 4. XPS results for calcined samples.

Proba	B.E. (eV)		ΔE_{sat} (eV)		Co/Si ^a	Ni/Si ^a
	Co 2p _{3/2}	Ni 2p _{3/2}	Co	Ni		
CoNi01	-	855.60	-	6.0	-	0.0232 (0.0610)
CoNi28	-	855.60	-	6.2	-	0.0090 (0.022)
CoNi55	780.58	855.38	-	5.9	0.0034 (0.0620)	0.0059 (0.0700)
CoNi82	779.91	-	6.5	-	0.0039 (0.0380)	-
CoNi10	n.d.					

^a atomic ratios at solid surface are shown in brackets

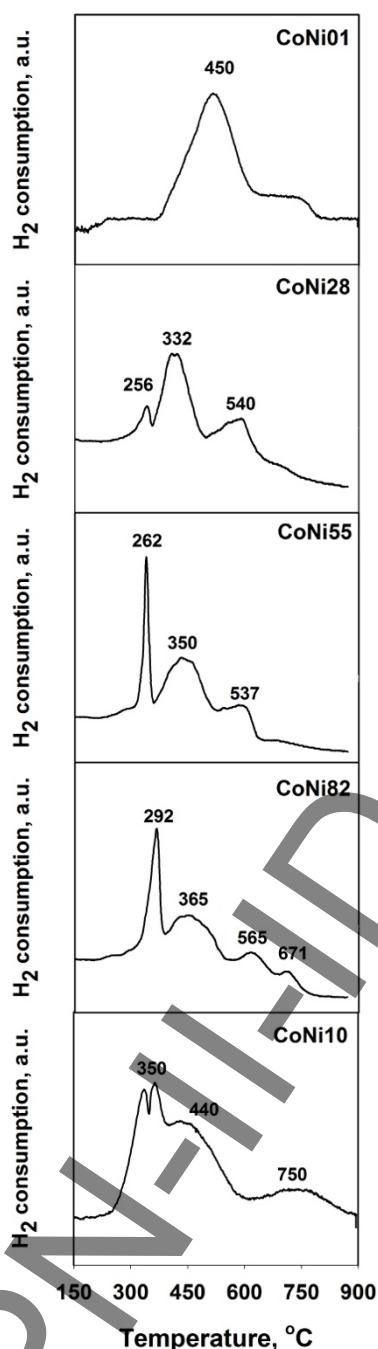


Fig. 2. TPR profiles for CoNi/SBA-15 samples.

Fig. 2 illustrates the TPR profiles for mono- and bi-component samples with Co and Ni. In the case of Cu(Ni) mono-component samples, these profiles are specific to the reduction of Ni²⁺, Co²⁺ and Co³⁺ from the nanoparticles of NiO and Co₃O₄, respectively, deposited on silica solid surface. If Ni/SBA-15 sample is considered, the reduction peak is large and symmetrical suggesting interactions between NiO and silica. However, the peak with maximum at 450°C indicates the preferential formation of NiO nanoparticles confined in mesopores, but having weak interaction with the silica support.^{4,5} In the case of Co/SBA-15 sample, the TPR profile shows two peaks which could be attributed to the successive reduction of Co₃O₄ to Co⁰ and another one placed at high temperatures corresponding to the reduction of Co²⁺ cations which are in strong interactions with the silica surface.^{6,7} For bi-component samples, the TPR profiles are more complex containing several reduction peaks between 250° and 800°C, attributed to the reduction of Ni and Co cations from (i) different oxide species such as Co₃O₄, NiO and NiCo₂O₄, (ii) being in different degrees of interaction with silica surface and (iii) from nanoparticles with different sizes.^{8,9}

The evolution of crystalline phases as well as their thermal stability during the reduction process was monitored by in situ XRD for all samples. Some representative diffractograms are shown in Fig. 3. It could be mentioned, all the diffractograms recorded contain two additional diffraction peaks (44.5° and 63.5°) due to the alloy of kantal used as samples holder.

For Ni-mono-component sample (CoNi01; Fig. 3A), one observes that the intensity of diffraction peak decreases as the reduction temperature increases, but when the reduction temperature reaches 450°C new reduction peaks appear around of 2θ ~ 44.5° and ~ 51.5°C, respectively (partially they are superposed on kantal peaks). The peaks are typically for (111) and (200) planes of metallic nickel (Ni⁰). An average size of crystallites of 5 nm was obtained by applying Scherrer's equation.

For Co mono-component sample, the diffractograms registered after reduction up to 350°C contain diffraction peaks typically for Co₃O₄. In agreement with TPR data, the reduction of trivalent cations from Co₃O₄ to form CoO takes place at 350°C, whose diffraction peaks were identified at this temperature of reduction. The increase of temperature favors the subsequent reduction of CoO to Co⁰, fact reflected by the decrease of intensity of the corresponding CoO peak until its disappearance that means

the complete reduction of these cations.

At the same time, new diffraction peak at $\sim 75^\circ$ appeared which is typically for metallic phase of Co^0 . The intensity of this peak slowly increases with temperature but it is too small in order to apply Scherrer's equation.

For bi-component samples (CoNi28, CoNi55, CoNi82), the diffractograms registered after each level of reduction temperature (up to 350°C) show diffraction peaks corresponding to the main phases of NiO , Co_3O_4 , CoO and NiCo_2O_4 . Once surpassed the temperature of 350°C , the diffraction peaks attributed to oxides disappear and new peaks corresponding to the metallic phases appear. Thus, for sample CoNi28 new peaks corresponding to Ni^0 were identified, for sample CoNi82 it was observed the appearance of the peaks corresponding to Co^0 , while for sample CoNi55 peaks for both metals were observed.

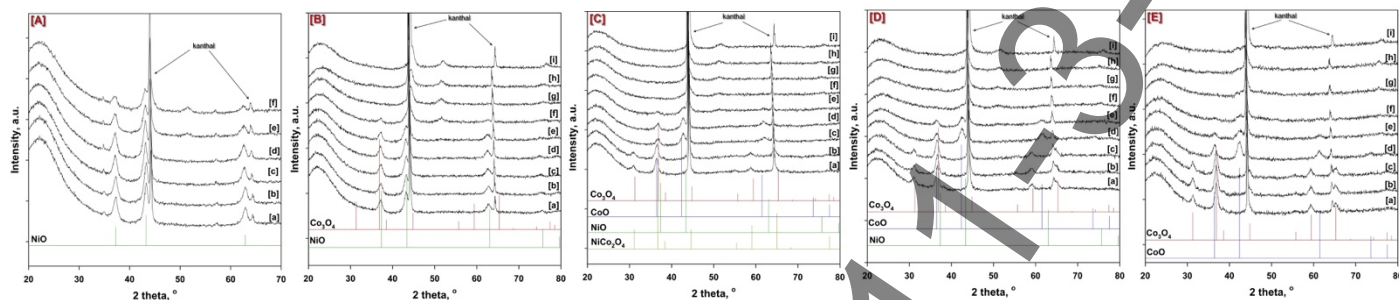


Fig. 3. XRD diffractograms registered in-situ after TPR at 30°C (a), 150°C (b), 250°C (c), 350°C (d), 450°C (e), 550°C (f), 650°C (g) and 750°C (h), after cooling under hydrogen at 30°C (i) for samples of CoNi/SBA-15 type: (A) CoNi01, (B) CoNi28, (C) CoNi55, (D) CoNi82, (E) CoNi10.

After the last reduction temperature of 550°C for CoNi01 and 750°C for other samples, TEM images have been recorded for the morphological analysis of metallic nanoparticles as well as for the analysis of their distribution inside pores. Some images are shown in Fig. 4.

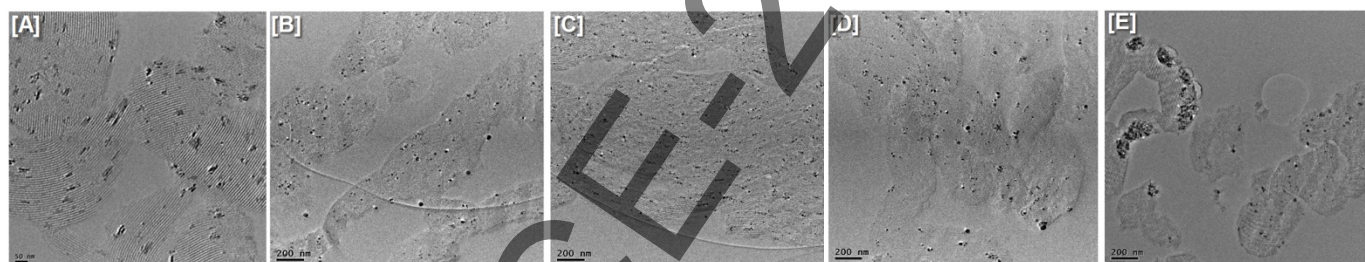


Fig. 4. TEM images for samples of CoNi/SBA-15 type after reduction at 500°C (Ni-mono-component) and 750°C respectively, for samples: (A) CoNi01, (B) CoNi28, (C) CoNi55, (D) CoNi82, (E) CoNi10.

As it can be observed from Fig. 4A, in the case of sample CoNi01 the nanoparticles of NiO are confined in mesopores without agglomerations and external phases. For sample CoNi10 (Fig. 4E) one observes two types of nanoparticles, namely: (i) particles of cobalt as big agglomerates inside of pores, this is possible due to the particular porous structure of SBA-15 silica where the primary mesopores are interconnected with micropores and secondary mesopores from porous wall, and (ii) particles of metallic cobalt very well dispersed inside support mesopores.⁷ For the bi-component samples, an improvement of the NPs distribution inside the mesopores besides the decreasing of their size are obvious, with a maximum at weight ratio between the two metals at 1:1. This result is in well agreement with high angle XRD after thermoprogrammed reduction as well as XRD and TEM for the oxide form of the samples, for which mixed oxide of NiCo_2O_4 type were noted at mass ratio = 1:1, whose reduction inside the mesopores of SBA-15 silica generates highly dispersed metallic NPs on the support surface.

O2/ Evaluation of the catalytic properties of materials in the hydrogenation of cinnamaldehyde.

A2.1. Hydrogenation of cinnamaldehyde in the presence of CoNi/SBA-15 catalysts at atmospheric pressure.

A2.2. Hydrogenation of cinnamaldehyde in the presence of CoNi/SBA-15 catalysts at higher pressures.

The cobalt- and nickel-based catalytic materials have been tested in the liquid phase hydrogenation of cinnamaldehyde under two different conditions of reaction: (i) at atmospheric pressure and 150°C , and (ii) at 10 bars and 130°C . The results obtained clearly point out the strong influence of the reaction conditions as well as the strong influence of nickel on the catalytic activity and selectivity of bi-metallic materials.

(i) Results of the catalytic tests performed at atmospheric pressure and 150 °C

Fig. 5 shows the variation of cinnamaldehyde conversion and the distribution of reaction products vs. reaction time as well as the initial reaction rates for each sample submitted to the catalytic tests at atmospheric pressure and 150 °C. From Fig. 5A it could be observed that the catalytic activity of mono-metallic Co-based catalyst is quite small, ~18 mole % after 360 min of reaction time, while the mono-metallic Ni-based catalyst leads to a conversion of 100 % only in 180 min. For the bimetallic samples, it was observed the same behavior as for Ni, irrespective of its content in catalyst. Thus, the total conversion of cinnamaldehyde took place in 300 min for all three bimetallic samples. Comparing these results with the previously reported in the literature, one observes an improved catalytic activity of the bimetallic solids from this research project. For instance, in the case of CoNi loaded on graphite (GRA), carbon nanotubes (MWCNT) and activated carbon (AC), atomic ratio Co:Ni = 1:1, the following conversion for the hydrogenation of cinnamaldehyde in ethanol, at 150 °C and 5 atm, were reported: 29.8 % (300 min of reaction time, CoNi/GRA), 62.6 % (480 min, CoNi/MWCNT) and 63.2 % (570 min, CoNi/AC), respectively.¹⁰

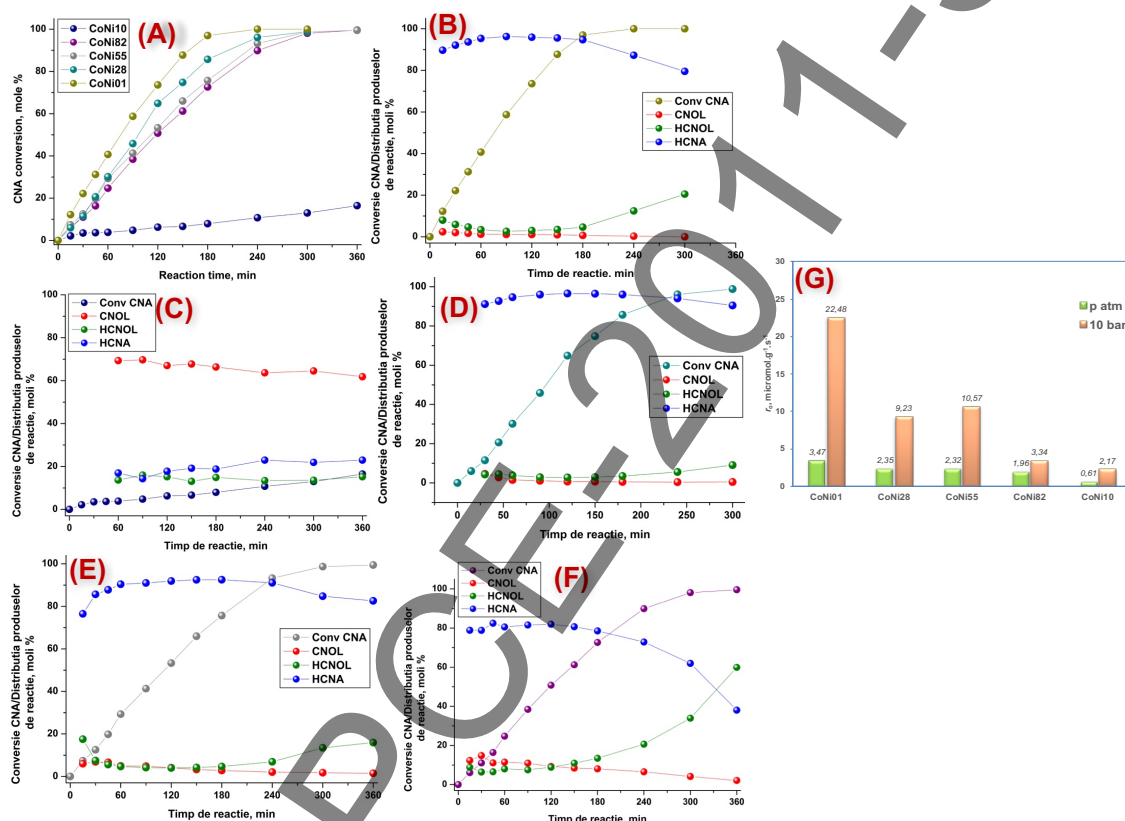


Fig. 5. CAN conversion vs. Reaction time (A), conversion and distribution of reaction products for CoNi01 (B), CoNi10 (C) CoNi28 (D), CoNi55 (F) and CoNi82 (F); Initial reaction rate for the catalysts of CoNi/SBA-15 type under both reaction conditions (G) (Atmospheric pressure, $T_{reduction} = 500$ °C; $T_{reaction} = 150$ °C, 0.265 g catalyst; 1 mL CNA, 25 mL propylene carbonate as solvent, H_2 flow rate = 1 L h⁻¹, speed rate = 900 rpm).

As the catalytic tests show, in the case of the mono-metallic catalysts (Co, Ni), the hydrogenation of CNA follows the reaction routes specific to each metal. Thus, in the case of Ni-base catalysts, the olefinic C=C bond is preferentially hydrogenated obtaining HCNA as main product (Fig. 5B), while the Co-based catalysts preferentially hydrogenates carbonyl group, C=O, forming CNOL as major product (Fig. 5C). The gradual introduction of nickel in catalyst composition provokes changes in the organic substrate adsorption so that the olefinic group is preferentially adsorbed and activated and the catalytic selectivity is directed towards HCNA, irrespective of the amount of nickel introduced in the catalyst formulation. However, the presence of cobalt atoms slightly influences the catalytic selectivity; therefore the amount of HCNA gradually decreases as the amount of cobalt increases. For instance, at 60 % conversion of CNA, the selectivity to HCNA decreases in the following order: 97 % (CoNi28) > 92 % (CoNi55) > 80 % (CoNi82).

This behavior indicates the fact that contrary to the case of bimetallic catalysts of CuNi and CuCo type, where an optimum ratio between the two metals was observed – when synergistic interactions between the two elements take place positively influencing both the physico-chemical and catalytic properties, for CoNi-based catalysts this phenomenon of synergism did not occur. It seems that for such catalysts, the changing of the adsorption way of CNA molecule on the catalyst surface, with effect on the selectivity, could be

controlled by a rational selection of the support. Indeed, recent studies shown that the deposition of such metals on carbon nanotubes (MWCNT – multi walls carbon nanotubes) favored an improved catalytic selectivity towards CNOL, even for metallic particles of ~ 5 nm.¹⁰ However, when these metals are deposited on graphite (GRA) or activated carbon (AC) the selectivity to CNOL is lower than in the previous case, though the size of metallic particle was greater (~ 18 nm – CoNi/AC, ~ 25 nm – CoNi/GRA), knowing that for cobalt higher selectivity to CNOL is expected when particle size is higher. Positive influence of carbon-based supports was also observed for Pd deposited on carbon nanotubes¹¹ or carbon fibers¹².

(ii) *Results of the catalytic tests performed at 10 bars pressure and 150 °C*

Fig. 6 illustrates the variation of CNA conversion and catalytic selectivity when the hydrogenation reaction is carried out at 10 bars.

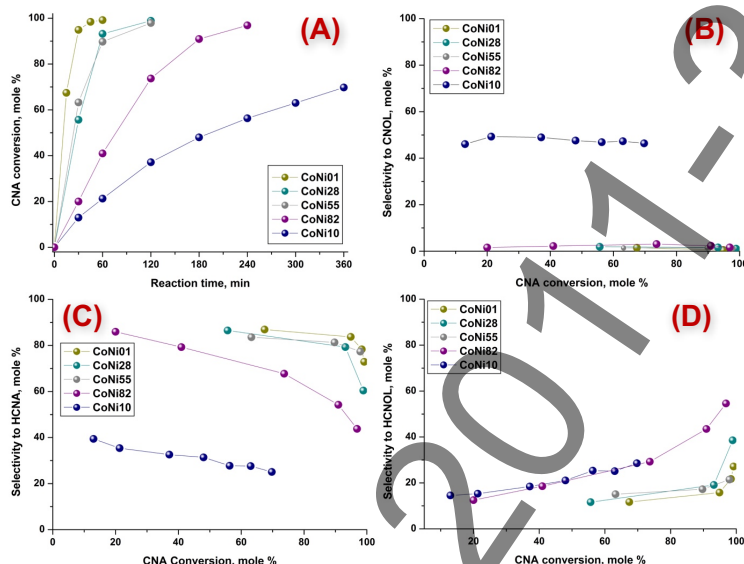


Fig. 6. Conversion of CNA as function of reaction time (A), selectivity to CNOL (B), HCNA (C) and HCNOL (D) for CoNi/SBA-15 catalysts. (Reaction conditions: $T_{reduction} = 500$ °C; $T_{reaction} = 130$ °C, 0.265 g catalyst; 1 mL CNA, 40 mL 2-propanol as solvent, pressure $H_2 = 10$ bar, speed = 700 rpm).

One observes that the catalytic activity, expressed as reaction rate (Fig. 5G), and CNA conversion (Fig. 6A) are significantly improved when the hydrogenation reaction is carried out under 10 bar in comparison to those obtained at atmospheric pressure, but the general trend as function of catalyst composition is not modified. The influence of higher pressure on the selectivity to CNOL is negative; it was lower by comparison with the results obtained at atmospheric pressure. It is worth to note that until now, it was reported that the pressure could have different effects on the selectivity to CNOL. Thus, increase, decrease or no effect on the selectivity were noticed when the pressure was increased. Also, it was observed that the nature of support could influence the selectivity when the reaction is carried out under pressure. For instance, a diminution of the selectivity to CNOL with the pressure was observed for Pt/SiO₂¹³, while by substitution of silica with graphite did not affected the selectivity¹⁴.

The original results obtained in this stage of the research project have been included in 2 papers in ISI quoted journals^{5,7} and constituted the subject of 4 scientific communications at international congresses.

Reference

1. Ungureanu, A.; Dragoi, B.; Chiriac, A.; Ciotonea, C.; Royer, S.; Duprez, D.; Mamede, A.S.; Dumitriu, E. *ACS Appl. Mater. Interfaces*, 2013, **5**, 3010
2. Venezia, A.M.; Murania, R.; Pantaleo, G.; Deganello, G. *J. Mol. Catal. A: Chem.*, 2007, **271**, 238.
3. Dumitriu, E; Raport stiintific privind implementarea proiectului PN-II-ID-PCE-2011-3-0868, (2015).
4. Habimana, F.; Li, X.; Ji, S.; Lang, B.; Sun, D.; Li, C. *J. Nat. Gas Chem.*, 2009, **18**, 392.
5. Chiriac, A.; Dragoi, B.; Ungureanu, A.; Ciotonea, C.; Mazilu, I.; Royer, S.; Mamede, A.S.; Rombi, E.; Italo, F.; Dumitriu, E., *J. Catal.*, 2016, **339**, 270.
6. Tsocheva, T.; Ivanova, L.; Rosenholm, J.; Linden, M. *Appl. Catal. B-Environ.*, 2009, **89**, 365.
7. Dragoi, B.; Ungureanu, A.; Ciotonea, C.; Chiriac, A.; Petit, S.; Royer, S.; Dumitriu, E., *Microporous and Mesoporous Mater.*, 2016, **224**, 176.
8. Luisetto, I.; Tuti, S.; Di Bartolomeo, E. *Int. J. Hydrogen Energ.*, 2012, **37**, 15992.
9. Pudukudya, M.; Yaakob, Z.; Akmal, Z. S. *Appl. Surf. Sci.*, 2015, **330**, 418.
10. Malobela, L.J.; Heveling, J.; Augustyn, W.G.; Cele, L.M. *Ind. Eng. Chem. Res.* 2014, **53**, 13910.
11. Ledoux, M. J.; Vieira, R.; Pham-Huu, C.; Keller, N. *J. Catal.* 2003, **216**, 333.
12. Pham-Huu, C.; Keller, N.; Ehret, G.; Charbonniere, L. J.; Ziessel, R.; Ledoux, M. J. *J. Mol. Catal. A: Chem.*, 2001, **170**, 155.
13. Shirai, M.; Tanaka, T.; Arai, M. *J. Mol. Catal. A: Chem.*, 2001, **168**, 99.
14. Koo-amornpattana, W.; Winterbottom, J.M. *Catal. Today* 2001, **66**, 277.